Three-Dimensional Asymmetrical Modeling of the Mitral Valve: A Finite Element Study with Dynamic Boundaries

Khee Hiang Lim[1], Joon Hock Yeo[1], Carlos M. G. Duran[2]

[1]*Nanyang Technological University, School of Mechanical and Aerospace Engineering, Singapore,* [2]*The International Heart Institute of Montana Foundation, Missoula, Montana, USA*

Background and aim of the study: **Previous computational studies of the normal mitral valve have been limited because they assumed symmetrical modeling and artificial boundary conditions. The study aim was to model the mitral valve complex asymmetrically with three-dimensional (3-D) dynamic boundaries obtained from in-vivo experimental data.**
Methods: **Distance tracings between ultrasound crystals placed in the sheep mitral valve were converted into 3-D coordinates to reconstruct an initial asymmetric mitral model and subsequent dynamic boundary conditions. The non-linear, real-time left ventricular and aortic pressure loads were acquired synchronously. A quasi-static solution was applied over one cardiac cycle.**
Results: **The mitral valve leaflet stress was heterogeneous. The trigones experienced highest stresses, while the mid-anterior annulus between trigones experienced low stress. High leaflet stress was observed during peak pressure loading. During isovolumic relaxation, the leaflets were highly stretched between the anterolateral trigone and the posteromedial commissure, resulting in a prominent secondary leaflet stress re-increment. This has not been observed previously, as symmetric models with artificial boundary conditions were studied only in the ejection phase.**
Conclusion: **Here, the first asymmetrical mitral valve model synchronized with 3-D dynamic boundaries and non-linear pressure loadings over the whole cardiac cycle based on in vivo experimental data is described. Despite its limitations, this model provides new insights into the distribution of leaflet stress in the mitral valve.**

The Journal of Heart Valve Disease 2005;14:386-392

Numerical study of the mitral valve includes both mathematical modeling and computational simulation. Although mathematical formulations of the mitral valve are not new (1-4), the valve's complex structure has limited modeling to a two-dimensional cross-section through the center of the anterior and posterior leaflets. The valve was assumed to be symmetrical, linear, and with cylindrical or ellipsoidal leaflet curvatures (1), but unfortunately these anatomically incorrect assumptions resulted in contradictory findings between the modeling and the physiological observations (5-7).

The complex mitral valve apparatus includes the annulus, leaflets, chordae tendineae, papillary muscles and left ventricular (LV) myocardium, and the disorder of any of these components will affect valve function. At a time when mitral valve repairs are being widely applied, an engineering perspective of normal valve function is highly desirable. Modeling of the mitral valve helps not only in understanding the mechanics and function of the valve, but also in alerting the surgeon to maneuvers that increase or reduce regions of stress concentration (8-14).

Whilst many cardiac valve modeling studies have focused on the aortic valve because of its relatively symmetrical geometry and uniformity, the highly complex mitral valve makes modeling far more difficult and tedious. Kunzelman et al. (8) first developed a 3-D finite element model of the normal mitral valve, this being based on static data from excised porcine mitral valves which were assumed to be similar to the human valve (15). Black et al. (12) have shown that the exclusion of bending stress in the leaflets will induce significant errors, and concluded that there was a need for an element which is able to simulate both bending and

Presented as a poster at the Second Biennial Meeting of the Society for Heart Valve Disease, 28th June-1st July 2003, Palais des Congrès, Paris, France

Address for correspondence:
Joon Hock (Tony) Yeo PhD, Nanyang Technological University, School of Mechanical and Aerospace Engineering, 50, Nanyang Avenue, Singapore 639798, Singapore
e-mail: mjhyeo@ntu.edu.sg

membrane stresses. Patterson et al. (13) compared linear and non-linear material properties for the leaflets, and found that the latter to simulated much better the valve closure process than the former.

None of the available finite element models is asymmetrical. All have been modeled symmetrically about the midline of the anterior and posterior leaflets. Some authors have used isotropic (12,13) material properties, whilst others used orthotropic properties (8), though all were obtained from either bovine pericardium or porcine valves. To date, no human mitral valve mechanical properties have been used in such an analysis. The originality of the present asymmetrical finite element mitral valve model is the asymmetric dynamic boundaries synchronized with non-linear pressure loads obtained from experimental animal data.

Materials and methods

Animal surgical protocol and coordinates data acquisition

The detailed surgical protocol used has been reported previously (16). Under cardiopulmonary bypass (CPB), 12 transceiver crystals were placed in the mitral valve (Fig. 1). After CPB was discontinued and the animal was hemodynamically stable (at least 15 min), distance tracings of all crystals were recorded at 200 Hz using a Sonomicrometer (Sonometrics Corp., London, ON, Canada). The synchronized real-time LV and aorta pressures were recorded using high-fidelity, catheter-tipped pressure transducers (model 510; Millar Instruments, Houston, TX, USA) placed through the LV apex and in the left ventricle and ascending aorta.

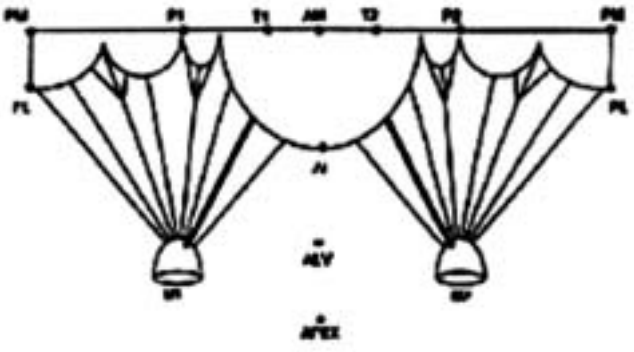

Figure 1: Positioning of the transceiver crystals in an open mitral valve apparatus sectioned along the middle of posterior leaflet. A total of 12 crystals was placed on the apparatus: anterior and posterior trigones (T1, T2); midpoint of anterior and posterior annulus (AM, PM); left and right lateral extremities of the insertion of the posterior leaflet (P1, P2); tip of each papillary muscle at the insertion of the anterior leaflet's basal chordae (M1, M2); free edge of the middle part of the anterior leaflet and the middle scallop of the posterior leaflet (AL, PL); anterior septum of left ventricle wall (ALV) and apex.

3-D coordinates reconstruction

A post-processing program (SonoSOFT, Version 3.1.4; Sonometrics Corp.) was used to process the length tracings between crystals. The 3-D reconstruction of the crystal coordinates over a cardiac cycle was carried out using SonoXYZ (Version 1.0.12, Sonometrics Corp.). The apex was selected as the origin of the coordinate system.

The Sonomicrometer was operated at 200 Hz; thus, for a cardiac cycle of 0.615 s, a total of 124 data sets was recorded. This began with time zero at end-diastole and increased by time step intervals of 0.005 s; hence, a total of 123 steps was recorded.

3-D asymmetrical mitral valve modeling

Computer-aided design (CAD) software (Pro/Engineer 2000i; Parametric Technology Corp., MA, USA) was used to create the initial model, which was based on the coordinates of the 12 crystals at end-diastole. The apex was used as the origin center. A spline curve was fitted through the six crystals placed around the mitral annulus. The coordinates of the two papillary muscle tips were used directly. The leaflet edge was assumed as a curve passing through free edge crystals, while the body of the anterior and posterior leaflets (between annulus and leaflet edge) was modeled as two spline surfaces (units for the model were expressed in millimeters). The entire valve was asymmetrical with twisted, saddle-shaped mitral annulus geometry. The completed model was exported in Initial Graphics Exchange Specification (IGES) format before being imported into ANSYS for further processing.

Model assumptions

The CAD model was imported into ANSYS 5.7 Mechanical University High Version (ANSYS Inc.,

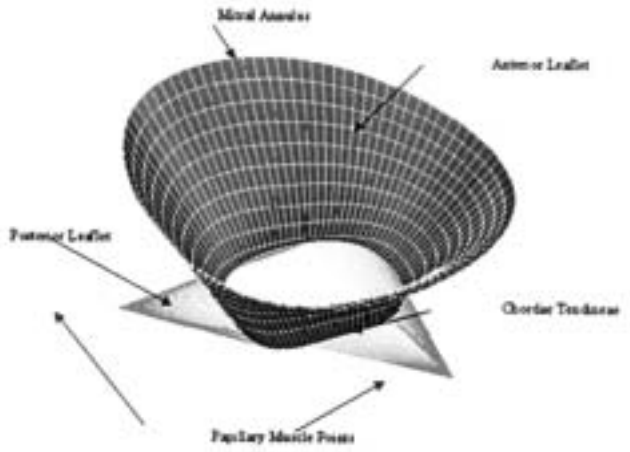

Figure 2: Complete mitral valve modeling with chordae tendineae.

J Heart Valve Dis
Vol. 14. No. 3
May 2005

Canonsburg, PA, USA) that runs on SGI Origin 2000. The mitral valve has been reported to operate continuously under tension and in the post-transition region, where the modulus of elasticity does not vary widely (17,18). Thus, the mitral valve was assumed to have linear isotropic properties.

The previously reported post-transition moduli of the leaflets ranged between 0.83 and 9.0 MPa (19-21), an almost 11-fold variation. This large range may be due to the high variation in valve thickness from annulus to belly to leaflet free-edge, and to the fiber orientation that most likely were not taken into consideration. Because the fibrous trigones have a higher modulus than the thin belly, it would be more conservative to use the lower modulus for leaflet modeling. Thus, both leaflets were assumed to have the same elastic modulus of 0.8 MPa. A Poisson's ratio of 0.45 was assumed to approach the incompressible behavior of the biological tissue (8). Also, because the mitral valve thickness ranges from 0.5 mm at the leaflet belly to almost 2 mm at the fibrous trigones, the assumption was made that both leaflets had an average constant thickness of ~1.26 mm (8). The mitral annulus was represented by nodes at the insertion point of the leaflets without specific material properties. Similarly, the papillary muscles were represented by a single node with no associated material properties.

Shell element (SHELL181) was selected to represent the leaflet surfaces. Since the annulus and papillary muscle points were represented by nodes, no specific element was assigned to these representations.

Mesh size

In order to determine the optimum mesh size that would ensure accuracy of results and reasonable computation time and costs, a simple comparison was carried out to determine the optimum mesh size, with material properties settings exactly as for the final model. The boundary conditions were simplified. The mitral annulus was fixed with only rotational displacement about all axes permitted. The leaflet edge was free to rotate about any axis, but constrained in the positive x-direction for a displacement of 1 mm. The maximum pressure load applied was 0.009046 MPa (equivalent to 68 mmHg), which was recorded in the animal experiments. The model was solved for 10 different mesh sizes between 50 and 8,000 elements, and the computation time and displacement accuracy were recorded and compared.

At least 500 elements were required to obtain accuracy within 2% error and short computational time (0.11 h), but abrupt element bends were found. In order to prevent a marginally acceptable mesh size limit of 500 elements, and to improve the model curvature with greater accuracy, a 1,000-mesh size model was used with 100 equal distance nodes along the annulus ring and leaflet edge (100 columns) and 10 equal distance nodes from the annular attachment to the free-edge (10 rows). Since the mitral annulus and papillary muscles were represented by nodes, no meshing could be associated with these representations.

Generation of chordae tendineae and contact element

A tension-only or compression-only spar, LINK10, was chosen to model the chordae tendineae. In the current analysis, only the marginal chordae were modeled. The chordae were assumed to have a uniform cross-section of 0.8 mm^2 (22), with an elastic modulus of 132 MPa. The coefficient of friction between leaflets was set to zero ($\mu = 0$) so that the leaflets were free to slide against one another during contact simulation.

Generation and application of moving boundaries

A spline curve was fitted through the six annular crystals before being interpolated into 100 equal intervals and used as the first displacement constraint. The same procedures were performed to generate the subsequent moving boundaries of the annulus over the cardiac cycle. The generated 3-D coordinates of the interpolated points were then corresponded to the 100 nodes on the mitral annulus to serve as the moving boundaries from step to step.

The converted 3-D coordinates of papillary muscles were used directly, as the moving boundaries as the papillary muscles were modeled as points. The nonlinear LV pressure loads were used directly, as the applied pressure loads on the ventricle side of the mitral leaflets. All pressure loads always act perpendicular to the element surface and follow the element rotation. The leaflet free-edge was only restrained by pulling of the chordae tendineae.

Solution method

Every step was a static large deformation analysis with variable sub-steps. The end time for each load step was prescribed according to the time-step increment. As the contact elements were non-linear and the large deformation solution required continuous update of structural stiffness matrix reformulation to achieve accurate convergent, a full Newton-Raphson method was employed. This method is suitable for a large deformation body where the structural stiffness matrix based on the initial geometry can no longer characterize the deformed structure. Each step interval was solved statically, but the combined results gave the quasi-static solution.

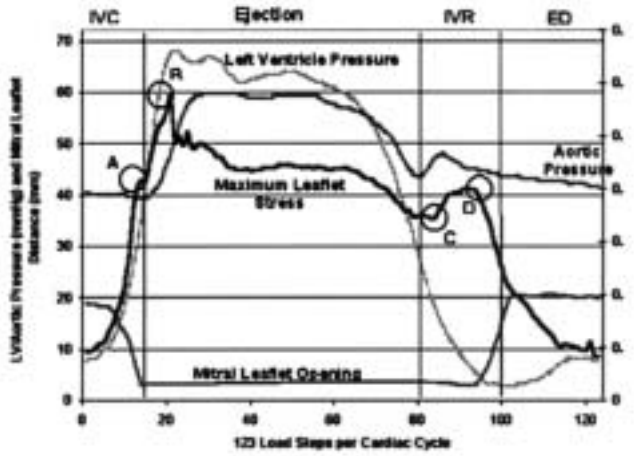

Figure 3: Maximum leaflet stress plot against left ventricular (LV) pressure, aortic pressure and mitral leaflet opening distance over a cardiac cycle. The mitral leaflet opening curve shown in the graph was acquired from animal experiment data. See text for details of points A, B, C and D.

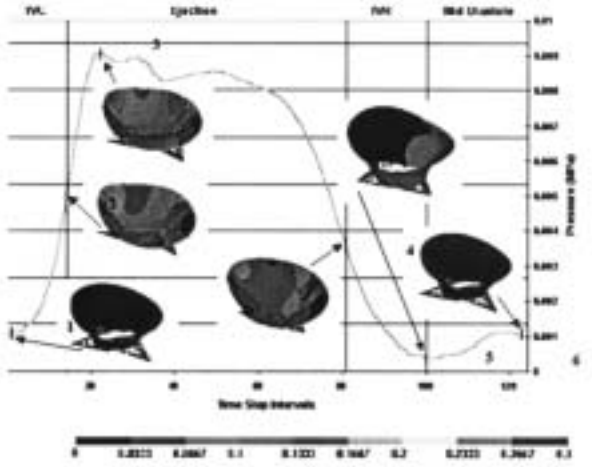

Figure 4: Contours of von Mises stress on the deformed mitral valve at various times of the cardiac cycle. All models have a similar color code in MPa for effective comparison.

Results

Maximum leaflet stress

The simultaneous analysis of the von Mises stress pattern of the mitral valve, together with the LV pressure tracing, is shown in Figure 3. Both the pressure and stress curves were similar during the isovolumic contraction (IVC) and rapid ejection phases. The curves increased drastically, reaching peak values at early ejection (Fig. 3, point B), followed by a plateau before the end of ejection when both the LV pressure and valve stress began to decrease. During IVC, the mitral valve was still open, and achieved complete closure only at the end of IVC. The mitral stress increased in parallel with the LV pressure build up until the aortic valve opening at end IVC induced a sudden release of leaflet stress (shown as point A in Fig. 3).

During early isovolumic relaxation (IVR), the leaflet stress curve was flat, but this was soon followed by a stress re-increment (Fig. 3, point C). It has been shown (24) that complete aortic valve closure occurs slightly after the start of IVR. At that time point, the left ventricle relaxed isovolumically and skewed the mitral leaflets, causing the stress to build up from point C to D (see Fig. 3) when the mitral valve began to open. This valve opening corresponded with a rapid stress reduction that continued throughout the remaining end-diastole.

Leaflets stress distribution profiles

The leaflet deformations and stress distribution profiles were examined at various critical load steps across the cardiac cycle. In total, six load steps were selected for analysis (Table I). von Mises stress distribution profiles of the mitral valve were plotted as color stress contours on the deformed surface of the leaflets (see Fig. 4). The leaflet stress range of different regions of the valve is shown in Table II.

At the start of IVC (point 1 in Fig. 4), the anterior leaflet experienced slightly higher stress than the posterior leaflet (see Table II). Although the posterior belly has higher stress than the anterior belly, the posterior leaflet has an even stress distribution. At the end of IVC (point 2 in Fig. 4), the posterior leaflet began to

Table I: Corresponding load steps, pressure values and time intervals of Figure 4.*

Load step	Time (s)	Pressure (kPa)	Pressure (mmHg)	Point on Fig. 4
1	0.005	1.025	7.68	1
15	0.075	5.363	40.20	2
21	0.105	8.980	67.31	3
81	0.405	3.524	26.41	4
100	0.500	0.367	2.75	5
123	0.615	1.025	7.68	6

*Pressure loads quoted were obtained from animal experiments.

J Heart Valve Dis
Vol. 14. No. 3
May 2005

Table II: von Mises stress range over different sections of leaflets.

Leaflet area	von Mises stress range (MPa)					
	Point 1	Point 2	Point 3	Point 4	Point 5	Point 6
Anterolateral trigone (T1)	0.005~0.029	0.032~0.132	0.012~0.151	0.016~0.103	0.001~0.015	0.006~0.028
Posteromedial trigone (T2)	0.007~0.027	0.054~0.128	0.087~0.173	0.033~0.081	0.026~0.039	0.009~0.026
Middle of anterior annulus (AM)	0.008~0.018	0.034~0.078	0.045~0.110	0.027~0.046	0.011~0.027	0.008~0.015
Anterior belly	0.010~0.021	0.056~0.094	0.074~0.120	0.030~0.054	0.010~0.023	0.010~0.016
Anterior leaflet	0.002~0.032	0.034~0.135	0.045~0.173	0.016~0.122	0.001~0.065	0.002~0.031
Anterolateral commissural (P1)	0.004~0.026	0.056~0.109	0.049~0.120	0.020~0.085	0.042~0.067	0.002~0.017
Posteromedial commissural (P2)	0.002~0.022	0.002~0.072	0.005~0.070	0.015~0.036	0.042~0.077	0.002~0.019
Middle of posterior annulus (PM)	0.003~0.025	0.029~0.098	0.070~0.112	0.043~0.065	0.055~0.070	0.003~0.022
Posterior belly	0.007~0.025	0.039~0.109	0.086~0.139	0.057~0.099	0.053~0.083	0.007~0.022
Posterior leaflet	0.003~0.024	0.020~0.139	0.017~0.145	0.011~0.131	0.039~0.098	0.002~0.024
Leaflet edge	0.001~0.046	0.029~0.205	0.053~0.266	0.006~0.170	0.002~0.123	0.001~0.042

fold up and move towards the anterior leaflet to close the valve. The natural redundancy (multiple folding) of the posterior leaflet for valve closure was pronounced. The trigones and leaflet edge were the main regions of stress concentration (Table II). The mitral annulus slowly skewed clockwise towards the left, while the anterior papillary muscle moved towards the right. As a result of stretching and twisting, the P1 stress region was higher than the P2 stress region, where the leaflet became crumpled.

During the maximum pressure load (point 3 in Fig. 4), both trigones experienced high stresses, though maximum stress occurred at the leaflet edge. The anterior leaflet remained relatively flat, but major bending was observed near the posterior belly to close the valve. Natural redundancy of the posterior leaflet was prominent, and the valve was skewed along the T1 and P2 directions. The stress at the P2 area was low due to crumpling of the tissue at this region. The stress at the posterior belly was higher than at the anterior belly, despite the anterior leaflet having a higher stress on average. The stress at the AM region was relatively low compared to that of the trigones and anterior belly. In addition, a progressive annular stress increment was observed from the P2 region towards the PM region and the P1 region.

Valve skewing remained prominent along the T1-P2 direction at the end of systole (point 4 in Fig. 4), despite the low pressure. The posterior belly was stretched diagonally along the T1-M2 direction, causing stress which was almost two-fold greater than that in the anterior belly. The lowest stress occurred around the P2 region, due to extra tissue crumpling. However, at the end of IVR (point 5 in Fig. 4), the leaflet was mainly stressed by skewing of the leaflets along the T1-P2 direction, causing the stress distributions to become concentrated around the P2 region. The leaflet stress was progressively increased from T1 to AM to T2 and, similarly, from P1 to PM to P2. It should be noted that stress in the trigone region for all previous load steps was always higher than that in the commissural region; however, at the current load step, stresses at the trigones were far below those of the commissural regions, despite the trigones remaining as the high-stress regions of the anterior leaflet.

At end-diastole (point 6 in Fig. 4), the mitral valve moved back to its initial position of the cardiac cycle, so that it was ready for the next cycle to start. Therefore, the stress distribution profile was close to that in load step 1.

Discussion

Finite element modeling

Both radiography (25-29) and echocardiography (30-32) have been used intensively to study the dynamics of the mitral valve. Whilst the low sampling rate (60 Hz) of these techniques has restricted application of the data into modeling and boundary conditions, the high sampling rate (200 Hz) of sonomicrometry offers a new approach to study 3-D mitral valve dynamics.

The unique nature of the present model relates to the use of real-time 3-D coordinates at the dynamic state (end-diastole). All previous geometric modeling has been carried out with geometric profiles captured at static state, where the heart is not beating. Previous studies used either pressurized excised hearts to capture images, or hearts sliced into thin layers (8), before reconstructing the initial valve geometry. In addition, these excised hearts may be distorted by the artificial holding devices. The use of dynamic coordinates in the present study indicated that the valve is totally asymmetrical, with a twisted, saddle-shape annulus geometry. Although symmetrical modeling saves computing power, time and costs, and has a better convergence rate, the asymmetrical model provides more accurate results.

Another important input parameter to ensure accuracy is that of applied boundary conditions. All previous studies have used artificial boundary conditions,

or have assumed linear pressure loadings (8). The actual mitral valve motion is highly complex, and involves irregular twisting and skewing. The 3-D dynamic coordinates obtained using sonomicrometry have shown that the annulus and papillary motions are 3-D in the atrioventricular chamber; therefore, such experimental boundary conditions and pressure loads were critical for effective modeling of any twisting or pulling of the mitral valve during simulation.

Although most previous studies have simulated only the systolic period, the second half of ejection towards end-diastole can be equally important, since relaxation of the active muscles produces movements that will introduce twisting and skewing of the leaflets, thereby causing interesting variations in stress over the leaflet. The results of the present study have shown that the valve is highly skewed towards the end of IVR, which will not be identified if diastole is not simulated.

Previous studies quoted material properties either from porcine valves or bovine pericardium (8,12,13). The present study is the first finite element model to use human material properties for all valve components.

Finite element analysis

As in previous studies (8), the two high-stress regions found in the current model were the trigones and the leaflet edge. However, the trigone stress fell below that of the posteromedial commissural region during the end of IVR, due to skewing of the leaflets by muscle relaxation - a finding which has not previously been reported. The mid-point of the annulus between the high-stress trigones has relatively low stress, most likely because of the highly asymmetrical saddle-shape of the annulus. The leaflet edge is connected by the chordae tendineae, which are concentration nodes, and this - together with multiple folding of the leaflet edge - introduces high bending stresses.

Whilst it is known that the anterior leaflet plays a major role in valve closure (8), the results of the present study showed that the posterior leaflet also moves substantially, with high bending at its belly, towards the anterior leaflet. The active annulus muscles around the posterior region are responsible for the large posterior movement towards the anterior leaflet. The anterior leaflet moved with a relatively flat surface towards the posterior leaflet, whereas the posterior leaflet bent and curved towards the anterior leaflet to coordinate the valve closure process. Although this substantial movement of the posterior leaflet has not been reported in any previous investigation, the natural redundancy found at the posterior leaflet agrees well with previous findings (8).

Two major improvements have been incorporated into the current finite element model, namely the asymmetrical modeling and the real time 3-D dynamics boundaries synchronized with non-linear pressure loads. Despite these assumptions and quasi-static solution, the results of the simulation have inevitably further explored the insights of the dynamics of the mitral valve.

Study limitations

With regard to finite element modeling, a major limitation was the assumption of a flat leaflet edge. In fact, the leaflet edge is highly undulating, so that full modeling would require many crystals to be implanted on the leaflet edge, and this would impair natural movement. Although the leaflet edge can be assumed from a previous mitral valve anatomy study (15), this is incompatible as a dynamic sheep model was not used. The insertion for the marginal chordae is clearly along the leaflet edge, whereas basal chordae insertion is random and further back from the leaflet edge. The marginal chordae were also found to outnumber the basal chordae by two to one; hence, removal of the latter would not seriously compromise mitral valve function as the marginal chordae carry a greater stress load than the basal chordae (27). Thus, only the marginal chordae were modeled in the current study.

With regard to finite element analysis, progress in mitral valve modeling has been limited to symmetrical modeling and artificial boundary conditions, due mainly to a lack of experimental animal data. These data form the mainstay of the present study, and should represent a step forward in the understanding of mitral function. Actual overall stress distribution on the mitral valve leaflets in vivo was not available for comparison with the present predicted finite element results because of the assumed linear isotropic properties and uniform thickness which might be artificially high, but consistent with previous research findings (8). Due to the present limited availability of state-of-the-art instrumentation, accurate measurement of the entire stress pattern of the mitral valve complex in vivo may be extremely difficult.

Acknowledgements

The authors thank Jill Roberts for her editorial assistance, and are grateful to the Center for Advanced Numerical Engineering Simulation (CANES), Nanyang Technological University (NTU), Singapore, for providing the computing resources. These studies were supported by the School of Mechanical and Aerospace Engineering, NTU.

References

1. Arts T, Meerbaum S, Reneman RS, Corday E. Stresses in the closed mitral valve: A model study. J Biomech 1983;16:539-547
2. Mazumdar J, Hearn TC. Mathematical analysis of

mitral valve leaflets. J Biomech 1978;11:291-296
3. Arts T, Reneman RS. Dynamics of left ventricular wall and mitral valve mechanics - A model study. J Biomech 1989;22:261-271
4. Miller GE, Hunter JF, Lively WM. A note on mitral valve mechanics: A pre-stressed leaflet concept. J Biomech 1981;14:373-375
5. Pohost GM, Dinsmore RE. The echocardiogram of the anterior leaflet of the mitral valve. Correlation with hemodynamic and cineroentgenographic studies in dogs. Circulation 1975;51:88-97
6. Priola DV, Fellows C, Moorehouse J, Sanchez R. Mechanical activity of canine mitral valve in situ. Physiology 1970;219:1647-1651
7. Rubenstein JJ, Pohost GM. The echocardiographic determination of mitral valve opening and closure. Correlation with hemodynamic studies in man. Circulation 1975;51:98-103
8. Kunzelman KS, Cochran RP, et al. Finite element analysis of mitral valve. J Heart Valve Dis 1993;2:326-340
9. Kunzelman KS, Reimink MS, Cochran RP. Flexible versus rigid ring annuloplasty for mitral valve annular dilation: A finite element model. J Heart Valve Dis 1998;7:108-116
10. Reimink MS, Kunzelman KS, Cochran RP. The effect of chordal replacement suture length on function and stresses in repaired mitral valves: A finite element study. J Heart Valve Dis 1996;5:365-375
11. Kunzelman KS, Cochran RP. Hemi-homograft replacement of the mitral valve: A finite element model. In: Huysmans HA, David TE, Westby S (ed.), Stentless Bioprosthesis. Isis Medical Media, Oxford, 1999:31-38
12. Black MM, Howard IC, Huang X, Patterson EA. A three-dimensional analysis of a bioprosthetic heart valve. J Biomech 1991;24:793-801
13. Patterson EA, Howard IC, Thornton MA. A comparative study of linear and nonlinear simulations of the leaflets in a bioprosthetic heart valve during the cardiac cycle. J Med Eng Tech 1996;20:95-108
14. Lim KH, Yeo JH, Sim EKW, Candra J, Duran CMG. Computational modeling of aortic valve mold models used for aortic valve reconstruction. The 10th Annual Meeting of the Asian Society for Cardiovascular Surgery. Jeju, Korea, 2002:Abstract #S10-06
15. Kunzelman KS, Cochran RP, Verrier ED, Eberhart RC. Anatomic basis for mitral valve modeling. J Heart Valve Dis 1994;3:491-496
16. Lansac E, Lim KH, Shomura Y, et al. Dynamic balance of the aortomitral junction. J Thorac Cardiovasc Surg 2002;123:911-918
17. Miller GE, Hunter JF, Lively WM. A note on mitral valve mechanics: A pre-stressed leaflet concept. J Biomech 1981;14:373-375
18. Rushmer RF, Finlayson BL, Nash AA. Movement of the mitral valve. Circ Res 1956;4:337-342
19. Clark RE. Stress-strain characteristics of fresh and frozen human aorta and mitral leaflets and chordae tendineae. Implications for clinical use. J Thorac Cardiovasc Surg 1973;66:202-208
20. Clark RE, Butterworth GAM. Characterization of the mechanics of human aorta and mitral valve leaflets. Surg Forum 1971;22:134-136
21. Ghista DN, Rao AP. Structural mechanics of the mitral valve: Stresses sustained by the valve; nontraumatic determination of the stiffness of the in vivo valve. J Biomech 1972;5:295-307
22. Barber JE, Ratliff NB, Cosgrove DM, III, Griffin BP, Vesely I. Myxomatous mitral valve chordae. I: Mechanical properties. J Heart Valve Dis 2001;10:320-324
23. Kunzelman KS, Cochran RP. Mechanical properties of basal and marginal mitral valve chordae tendineae. Am Soc Artif Intern Organs Trans 1990;36:M405-M408
24. Lansac E, Lim HS, Shomura Y, et al. A four-dimensional study of the aortic root dynamics. Eur J Cardiothorac Surg 2002;22:497-503
25. Komeda M, Glasson JR, Bolger AF, et al. Papillary muscle-left ventricular wall 'complex'. J Thorac Cardiovasc Surg 1997;113:292-301
26. Glasson JR, Komeda M, Daughters GT, et al. Three-dimensional regional dynamics of the normal mitral annulus during left ventricular ejection. J Thorac Cardiovasc Surg 1996;111:574-85
27. Karlsson MO, Glasson JR, Bolger AF, et al. Mitral valve opening in the ovine heart. Am J Physiol 1998;274(2 Pt.2):H552-H563
28. Glasson JR, Komeda M, Daughters GT, et al. Most ovine mitral annular three-dimensional size reduction occurs before ventricular systole and is abolished with ventricular pacing. Circulation 1997;96(9 Suppl.):II-115-II-122
29. Komeda M, Glasson JR, Bolger AF, et al. Three-dimensional dynamic geometry of the normal canine mitral annulus and papillary muscles. Circulation 1996;94(9 Suppl.):II159-II163
30. Kaplan SR, Bashein G, Sheehan FH, et al. Three-dimensional echocardiographic assessment of annular shape changes in the normal and regurgitant mitral valve. Am Heart J 2000;139:378-387
31. Flachskampf FA, Chandra S, Gaddipatti A, et al. Analysis of shape and motion of the mitral annulus in subjects with and without cardiomyopathy by echocardiographic 3-dimensional reconstruction. J Am Soc Echocardiogr 2000;13:277-287
32. Ormiston JA, Shah PM, Tei C, Wong M. Size and motion of the mitral valve annulus in man. I. A two-dimensional echocardiographic method and findings in normal subjects. Circulation 1981;64:113-120